Available online at www.sciencedirect.com
ScienceDirect
Journal of Power Sources 173 (2007) 346–356
JOURNAL OF POWER SOURCES
www.elsevier.com/locate/jpowsour

AC impedance modelling study on porous electrodes of proton exchange membrane fuel cells using an agglomerate model

Dietmar Gerteisen *, Alex Hakenjos, Jürgen O. Schumacher

Fraunhofer Institute for Solar Energy Systems, Heidenhofstr. 2, 79110 Freiburg, Germany

Received 16 March 2006; received in revised form 15 March 2007; accepted 29 April 2007
Available online 5 May 2007

Abstract

A one-dimensional model of the PEM fuel cell cathode is developed to analyse ac impedance spectra and polarisation curves. The porous gas diffusion electrode is assumed to consist of a network of dispersed catalyst (Pt/C) forming spherically shaped agglomerated zones that are filled with electrolyte. The coupled differential equation system describes: ternary gas diffusion in the backing (O_2, N_2, water vapour), Fickian diffusion and Tafel kinetics for the oxygen reduction reaction (ORR) inside the agglomerates, proton migration with ohmic losses and double-layer charging in the electrode. Measurements are made of a temperature-controlled fuel cell with a geometric area of 1.4 cm × 1.4 cm. Lateral homogeneity is ensured by using a high stoichiometry of λ_{min}. The model predicts the behaviour of measured polarisation curves and impedance spectra. It is found that a better humidification of the electrode leads to a higher volumetric double-layer capacity. The catalyst layer resistance shows the same behaviour depending on the humidification as the membrane resistance. Model parameters, e.g. Tafel slope, ionic resistance and agglomerate radius are varied. A sensitivity analysis of the model parameters is conducted.

Keywords: PEM fuel cell; Modelling; Agglomerate model; ac impedance spectroscopy; Oxygen reduction reaction; Tafel slope

1. Introduction

A proton exchange membrane (PEM) fuel cell is an electrochemical device in which the energy of a chemical reaction is converted directly into electricity. Hydrogen fuel is used in combination with air to produce electricity without combustion. The only by-products of the electrochemical reactions in the fuel cell are heat and water. Fuel cells are clean, quiet and energy-efficient. Possible application fields that are currently considered for PEM fuel cells include portable applications, stationary power generation and the automotive area. PEM fuel cells use a solid polymer membrane as electrolyte. The electrochemical reactions take place in porous gas diffusion electrodes.

Several processes are involved during fuel cell operation: the electrochemical reactions in the electrodes, transport of electrons and protons, mass-transport of the gas species and water, and heat transport. Electrochemical impedance spectroscopy is a powerful characterisation method to understand these complex processes in the fuel cell and electrodes, respectively. This measurement technique is based on the fact that the processes mentioned above take place on different characteristic time scales. Applying a small alternating voltage signal on a dc load level, the current response characterised by the amplitude and phase shift depends on the relaxation time of the coupled processes and thus on the perturbation frequency. The complex impedance is defined by the quotient of the perturbation voltage input and the ac current response. The impedance at different frequencies is called an impedance spectrum. The effects of the reaction kinetics, mass-transport processes and the limited ionic conductivity through the catalyst layer (CL) can be separated by analysing measured impedance spectra with a mathematical model.

Different approaches can be found in the literature to describe the dc and ac characteristics of a PEM fuel cell cathode. Mathematical models based on differential equations that describe the physics and the electrochemistry differ mostly in their geometrical properties. Springer et al. modeled the cathode as a homogeneous electrode and calculated polarisation curves [1]. Moreover, they presented a homogeneous cathode model for the calculation of ac impedance spectra [2]. Giner and Hunter

* Corresponding author. Tel.: +49 761 4588 5205; fax: +49 761 4588 9000.
E-mail address: dietmar.gerteisen@ise.fraunhofer.de (D. Gerteisen).

0378-7753/$ – see front matter © 2007 Elsevier B.V. All rights reserved.
doi:10.1016/j.jpowsour.2007.04.071

Nomenclature

b	Tafel slope (V)
c	total gas concentration in the backing (mol m^{-3})
c^*	concentration of the dissolved oxygen at the agglomerate surface (mol m^{-3})
c/c^*	normalised local oxygen concentration
$C_{DL,V}$	volumetric double-layer capacity (F m^{-3})
D	diffusion coefficient of dissolved oxygen in an agglomerate (m^2 s^{-1})
$\bar{f}$	Laplace-transformed function f
F	Faraday constant (9.6485×10^4 C mol^{-1})
i_0	exchange current density of the ORR at partial pressure of 1 atm (A m^{-2} atm^{-1})
i_0^V	$i_0\,\Gamma$, the product of the exchange current density of the ORR at partial pressure of 1 atm with the ratio of the active surface area inside an agglomerate per unit agglomerate volume (A m^{-3} atm^{-1})
j_{cell}	fuel cell current density (A m^{-2})
$j^r_{O_2}$	oxygen flux inside an agglomerate (mol m^{-2} s^{-1})
j^r_p	protonic current density inside an agglomerate (A m^{-2})
j^y_p	protonic current density in the catalyst layer
L	thickness of the catalyst layer (m)
n	number of transferred electrons
p_{O_2}	oxygen partial pressure (atm)
P_a	operating pressure (atm)
R_a	agglomerate radius (m)
R_{Ohm}	specific ionic resistance (Ω m)
s	Laplace-transform variable ($s = i\omega$)
T_{cell}	cell temperature (K)
x_{O_2}	molar fraction of oxygen
Z	impedance (Ω m^2)

Greek letters

ϵ_B	backing porosity
Γ	ratio of the active surface area inside the agglomerate to unit agglomerate volume (m^{-1})
η	overpotential (V)
Λ	product of the agglomerate surface area ($4\pi R_a^2$) and the density of the active agglomerates in the catalyst layer (m^{-1})
ω	angular frequency (s^{-1})

assumed that the catalyst material in the fuel cell electrode is contained within cylindrical agglomerates [3]. The cathode catalyst layer contains agglomerated zones, filled with electrolyte. The agglomerates are intercalated with open hydrophobic channels through which the oxidant reaches the surface of the flooded pores, dissolves, and diffuses to the catalyst particles, where the Faraday step occurs. Springer and Raistrick expanded this model for the simulation of ac impedance spectra [4]. However, SEM plots indicate that the assumption of spherically shaped agglomerates is more realistic for PEM fuel cell electrodes [5]. For simulating polarisation curves, agglomerates of spherical shape in the cathode electrode are assumed to be present in [6–8]. Jaouen and Lindbergh upgraded their steady-state agglomerate model to simulate ac impedance spectra [9]. For simplification, they neglected the gas diffusion limitation in the backing layer.

The mechanism of the oxygen reduction reaction in the fuel cell cathode is discussed by a number of authors. A doubling or even fourfold increase of the apparent Tafel slope has been reported and controversial interpreted. One explanation could be a change of the reaction mechanism. Damjanovic proposed the formation of several intermediate species during the oxygen reduction reaction (ORR) [10–12]. It is also well known that mass-transport limitations in the fuel cell cathode can cause a change in the apparent Tafel slope. When the cathode is controlled by the ORR and the diffusion of oxygen in the catalyst layer or by the ORR and the proton migration in the catalyst layer a doubling of the Tafel slope is observed [7]. An alternative explanation can be given by assuming spherical agglomerates in the electrode. According to this approach, the change of the Tafel slope is not caused by diffusion limitation of oxygen through the catalyst layer but by diffusion limitation of oxygen into the agglomerates [5,7,8].

In this paper, we present model-based analysis to extract physical and electrochemical parameters of the fuel cell cathode from impedance measurements. We developed a new cathode model based on the assumption of spherically shaped agglomerates. The model based on a coupled differential equation system describing: ternary gas diffusion in the backing (O_2, N_2, water vapour), Fickian diffusion and Tafel kinetics for the oxygen reduction reaction (ORR) inside the agglomerates, proton migration with ohmic losses and double-layer charging through the catalyst layer. The interaction between the electrode and the backing layer is taken into account for the calculation of ac impedance spectra and steady-state polarisation curves. Our model represents mass-transport limitation in the agglomerates as well as in the backing layer. The latter is significant at medium and high current density values and essential for simulating the behaviour of a PEM fuel cell in the whole current density range. According to our model, the change in the apparent Tafel slope is due to diffusion limitation of oxygen inside the agglomerates.

The model is used for a detailed analysis of mass-transport losses and losses due to the slow ORR in the cathode of a commercially available membrane electrode assembly from W.L. Gore & Associates (PRIMEA® Series 5510). We extract physical and electrochemical parameters by comparing measurement data and modelling results. Moreover, our cathode model can be used in more comprehensive mathematical models that include the fluid dynamics in the flow-fields.

2. Modelling

Our model takes into account both the structure of the electrode and the most important physical and electrochemical phenomena that occur in the electrode. These are the reaction kinetics of the ORR and the mass-transport limitation of oxygen caused by diffusion in the agglomerates. Furthermore, the model accounts for multicomponent gas diffusion in the backing layer. In particular, the interaction of the gas diffusion layer (GDL)

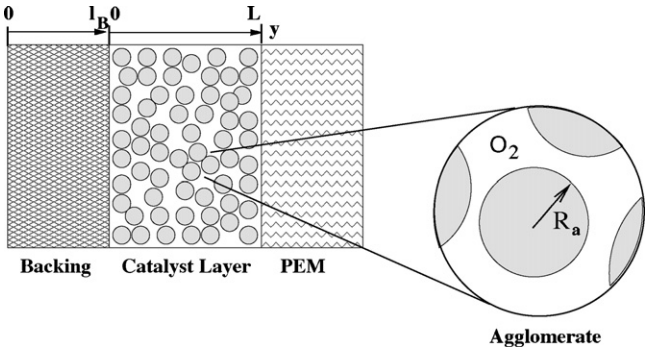

Fig. 1. Schematic diagram of the spherical agglomerate cathode model.

and the porous gas diffusion electrode of state-of-the-art PEM fuel cells is addressed.

The model considers only the cathode side of a PEMFC, losses on the anode side are neglected because of the small polarisation of a hydrogen electrode. The inner structure of the porous gas diffusion electrode is taken into account. In the catalyst layer, the dispersed catalyst (Pt/C) forms agglomerated zones filled with the electrolyte. These zones are surrounded by hydrophobic channels through which the reactant gases can diffuse. Agglomerates of mean radius R_a are assumed to be homogeneously distributed within the catalyst layer. Fig. 1 shows a schematic diagram of the cathode. A position-dependent activation overpotential is accounted for. The centre of an agglomerate determines its position within the catalyst layer. The size of the agglomerates is sufficiently small compared to the thickness of the active layer, so that an uniform overpotential within each agglomerate can be assumed.

The reactant gas dissolves in the bounded water of the ionomer at the boundary between the open gas pores and the agglomerates. Then the oxygen diffuses through the humidified electrolyte inside the agglomerates to the active sites where the electrochemical reaction takes place. The diffusion coefficient of the dissolved gas in the humidified electrolyte is about three orders of magnitude smaller than the diffusion coefficient of gas in the open pores. Hence, we assume that diffusion limitation in the open gas pores is negligible compared to diffusion losses within the agglomerates. Therefore, the oxygen concentration outside the agglomerates is set constant over the whole catalyst layer. Oxygen depletion occurs only inside the agglomerates where the electrochemical reaction takes place and in the backing layer due to mass-transport limitation.

At the moment this model does not describes the effects of liquid water. Thus, we are not able to predict flooding of the porous media or dehumidification of the ionomer. But these mentioned loss mechanisms can be interpreted by a change of model parameters like the effective porosity or the ionic resistance.

2.1. Gas transport in the backing layer

The model of the backing layer is based on the work of Springer et al. [2] where the equations are discussed in more detail. For better understanding, we review the most important assumptions and equations governing the gas transport in the backing layer.

Ternary diffusion of oxygen, nitrogen and water vapour occurs through the backing layer. Interdiffusion of these gases through the porous backing is calculated by means of the Stefan–Maxwell equation. Eq. (1) relates the instantaneous gradient of the oxygen mole fraction to the fluxes of oxygen, nitrogen and water vapour,

$$\frac{\mathrm{d}x_{\mathrm{O_2}}}{\mathrm{d}y} = [\alpha_{\mathrm{O_2}}(x_{\mathrm{O_2}}N_{\mathrm{w}} - x_{\mathrm{w}}N_{\mathrm{O_2}}) + x_{\mathrm{O_2}}N_{\mathrm{N_2}} - (1 - x_{\mathrm{O_2}} - x_{\mathrm{w}})N_{\mathrm{O_2}}]\frac{1}{cD_{\mathrm{eO_2N_2}}}, \quad (1)$$

where c and $\alpha_{\mathrm{O_2}}$ are given by

$$c = \frac{1}{\nu_{\mathrm{m}}}\frac{P_{\mathrm{a}}}{P_{\mathrm{S}}}\frac{T_{\mathrm{S}}}{T_{\mathrm{cell}}}, \qquad \alpha_{\mathrm{O_2}} = \frac{D_{\mathrm{SO_2N_2}}}{D_{\mathrm{SO_2w}}}. \quad (2)$$

A Bruggeman expression for $D_{\mathrm{eO_2N_2}}$ includes the effective porosity ϵ_{B} and the tortuosity τ of the gas diffusion layer:

$$D_{\mathrm{eO_2N_2}} = \frac{\epsilon_{\mathrm{B}}}{\tau}D_{\mathrm{SO_2N_2}}\left(\frac{T_{\mathrm{cell}}}{T_{\mathrm{S}}}\right)^{1.823}. \quad (3)$$

Here, x_i is the mole fraction of the gas species i, N_i is the molar flux of the gas i, D_{Sij} is the binary diffusion coefficient at standard conditions, T_{cell} is the cell temperature, $T_{\mathrm{S}} = 273.16\,\mathrm{K}$ is the standard temperature, $\nu_{\mathrm{m}} = 22.4 \times 10^{-3}\,\mathrm{m^3\,mol^{-1}}$ is the molar gas volume, c is the total gas concentration in the backing, P_{a} is the inlet pressure and $P_{\mathrm{S}} = 1$ atm is the standard pressure.

Equilibrium saturation of the cathode air stream with water vapour and isothermal conditions are assumed within the backing layer. Moreover it is assumed that the total pressure, i.e. the sum of the partial pressure of oxygen, nitrogen and water vapour remains constant inside the backing layer. Due to this constant total pressure within the backing layer the mole fraction of the water vapour is constant. Therefore, the gradient of water vapour in the backing layer vanishes in the Stefan–Maxwell equation:

$$\frac{\mathrm{d}x_{\mathrm{w}}}{\mathrm{d}y} = [\alpha_{\mathrm{O_2}}(x_{\mathrm{w}}N_{\mathrm{O_2}} - x_{\mathrm{O_2}}N_{\mathrm{w}}) + \alpha_{\mathrm{N_2}}(x_{\mathrm{w}}N_{\mathrm{N_2}} - (1 - x_{\mathrm{O_2}} - x_{\mathrm{w}})N_{\mathrm{w}})]\frac{1}{cD_{\mathrm{eO_2N_2}}} = 0, \quad (4)$$

where

$$\alpha_{\mathrm{N_2}} = \frac{D_{\mathrm{SO_2N_2}}}{D_{\mathrm{SwN_2}}}.$$

With an instantaneous ionic current density j_{cell}, there is an uniform molecular flux ($j_{\mathrm{cell}}/4F$) of oxygen and nitrogen through the backing layer. Thus the nitrogen flux can be replaced by the difference between $j_{\mathrm{cell}}/4F$ and the oxygen flux. With this substitution in Eq. (4), we can determine the water vapour flux N_{w} which is dragged along with the oxygen flux:

$$N_{\mathrm{w}} = \frac{x_{\mathrm{w}}\,N_{\mathrm{N_2}} + x_{\mathrm{w}}\,\alpha_{\mathrm{O_2}}/\alpha_{\mathrm{N_2}}\,(j_{\mathrm{cell}}/4F - N_{\mathrm{N_2}})}{1 - x_{\mathrm{w}} + (\alpha_{\mathrm{O_2}}/\alpha_{\mathrm{N_2}} - 1)\,x_{\mathrm{O_2}}}. \quad (5)$$

Inserting this water vapour flux in Eq. (1), we obtain an expression for the nitrogen flux:

$$N_{N_2} = \frac{cD_{eO_2N_2}}{l_B}\frac{1}{\beta_1}\left[\frac{j_{cell}}{i_B}(\beta_1 - x_{O_2}) + l_B G(x_{O_2})\frac{dx_{O_2}}{dy}\right], \quad (6)$$

where

$$G(x_{O_2}) = \frac{\beta_1 + \beta_2 x_{O_2}}{\beta_3 + \beta_2 x_{O_2}}, \quad \beta_1 = 1 - x_w,$$

$$\beta_2 = \frac{\alpha_{O_2}}{\alpha_{N_2}} - 1, \quad \beta_3 = 1 - x_w + \alpha_{O_2} x_w,$$

and the characteristic backing current density is given by $i_B = 4\,FcD_{eO_2N_2}/l_B$. The nitrogen flux throughout the backing layer N_{N_2} given by Eq. (6) is assumed to vanish under steady-state conditions because there is no nitrogen flux at the backing/catalyst layer interface. This leads to an implicit equation for the oxygen mole fraction at the interface backing/catalyst layer $x_{O_2}(l_B)$ as a function of the instantaneous ionic current density j_{cell} through the catalyst layer of the fuel cell:

$$\frac{j_{cell}}{i_B}y = \beta_4 \ln\left(\frac{\beta_1 - x_{O_2}(y)}{\beta_1 - x_{O_2}(0)}\right) + \beta_5 \ln\left(\frac{\beta_3 + \beta_2\, x_{O_2}(y)}{\beta_3 + \beta_2\, x_{O_2}(0)}\right), \quad (7)$$

where

$$\beta_4 = \frac{\beta_1(1+\beta_2)}{\beta_1\beta_2 + \beta_3}, \qquad \beta_5 = \frac{\beta_3 - \beta_1}{\beta_1\beta_1 + \beta_3}.$$

Although in our experiments the relative humidity of air at the inlet was clear under 100% (see below) the assumption of saturated air was made due to receive this implicit equation (Eq. (7)) for the oxygen mole fraction at the interface backing/catalyst layer and therefore a fast solution. Numerical calculations of the Stefan–Maxwell equation without these simplifications show that the error in the oxygen mole fraction at the interface is small by using the analytical solution given in Eq. (7). Moreover, the water generation of the ORR humidify the gas in the backing. Therefore, the relative humidity of air is not constant but a function of the current density. This feature and the related characteristics like water condensation or liquid water transport does not appear in the model.

2.2. The catalyst layer agglomerate model

The oxygen flux inside an agglomerate is modelled using Fick's first law:

$$j^r_{O_2}(r, y, t) = -Dc^*\frac{\partial}{\partial r}\frac{c(r, y, t)}{c^*}, \quad (8)$$

where $j^r_{O_2}$ is the oxygen flux inside a flooded agglomerate, D is the diffusion constant of dissolved oxygen within an agglomerate and c/c^* is the normalised local oxygen concentration with reference to the dissolved oxygen concentration on the agglomerate surface c^*. The oxygen mole fraction dissolved in water bounded in the ionomer, and consequently the dissolved oxygen concentration c^*, is calculated from the oxygen partial pressure p_{O_2} in the open gas pores using Henry's law:

$$x^{diss}_{O_2} = \frac{p_{O_2}}{K} = \frac{P_a x^{gas}_{O_2}}{K}, \quad (9)$$

where $K = 4.34 \times 10^4$ atm is the Henry constant [13]. The oxygen partial pressure can be calculated with the oxygen mole fraction at the backing/catalyst interface and the inlet pressure from the backing equations of Springer et al. [2].

The mass balance equation combines the local change of oxygen flux with oxygen consumption due to the ORR and the change of oxygen concentration with time:

$$\frac{1}{r^2}\frac{\partial}{\partial r}(r^2 j^r_{O_2}(r, y, t)) = -\frac{i^V_0\, p_{O_2}}{nF}\left(\frac{c(r, y, t)}{c^*}\right)\exp\left(\frac{2.3\,\eta(y, t)}{b}\right) - c^*\frac{\partial}{\partial t}\left(\frac{c(r, y, t)}{c^*}\right), \quad (10)$$

where r is the radial coordinate within an agglomerate. The volumetric exchange current density $i^V_0 = i_0\,\Gamma$ is the product of the exchange current density i_0 of the ORR at an O_2 partial pressure of 1 atm and the ratio Γ of the active surface area inside an agglomerate to unit agglomerate volume. It is difficult to extract Γ from measurements, so we use i^V_0 as a fit parameter. p_{O_2} is the oxygen partial pressure in the open gas pores of the catalyst layer, η is the overpotential and b is the Tafel slope. The boundary conditions are $(c(R_a, y, t)/c^*) = 1$ and $\partial/\partial r((c(0, y, t))/c^*) = 0$. Eqs. (8) and (10) determine the distribution of the normalised oxygen concentration inside the agglomerates depending on the local overpotential in the catalyst layer.

The proton flux inside an agglomerate j^r_p is given by the charge balance equation:

$$\frac{1}{r^2}\frac{\partial}{\partial r}(r^2 j^r_p(r, y, t)) = -i^V_0\, p_{O_2}\left(\frac{c(r, y, t)}{c^*}\right)\exp\left(\frac{2.3\,\eta(y, t)}{b}\right). \quad (11)$$

The boundary condition for Eq. (11) is that the proton flux in the centre of an agglomerate is zero: $j^r_p(0, y, t) = 0$.

At steady-state, the differential equations (8)–(11) yield the current density on the surface of an agglomerate $j^r_p(R_a, y)$ as a function of the position in the catalyst layer:

$$j^r_p(R_a, y) = \frac{nFDc^*}{R_a} - \sqrt{nFi^V_0\, p_{O_2} Dc^*\exp\left(\frac{2.3\,\eta(y)}{b}\right)} \times \coth\left(\frac{\sqrt{i^V_0\, p_{O_2}\exp(2.3\eta(y)/b)}R_a}{\sqrt{nFDc^*}}\right). \quad (12)$$

The charge balance equation along the y-direction is given by

$$\frac{\partial j^y_p(y, t)}{\partial y} = j^r_p(R_a, y, t)\Lambda + C_{DL,V}\frac{\partial \eta(y, t)}{\partial t}, \quad (13)$$

where the ionic current density at the surface area of an agglomerate is given by $j^r_p(R_a, y, t)$, and the agglomerate centre is located at position y in the electrode. $C_{DL,V}$ is the volumetric double-layer capacitance of the electrode and Λ is the product

of the agglomerate surface ($4\pi R_a^2$) and the density of the active agglomerates in the catalyst layer.

Ohm's law is used to calculate the overpotential distribution in the catalyst layer:

$$\frac{\partial \eta(y,t)}{\partial y} = R_{\mathrm{Ohm}}\, j_{\mathrm{p}}^{y}(y,t), \tag{14}$$

where R_{Ohm} is the specific ionic resistance of the catalyst layer. Due to the high electric conductivity of carbon compared to the low ionic conductivity of the ionomer, the ohmic losses in the carbon support are neglected. The proton flux at the interface between the backing layer and the active layer vanishes, leading to the boundary condition $j_{\mathrm{p}}^{y}(0,t) = 0$. The second boundary condition $j_{\mathrm{p}}^{y}(L,t) = j_{\mathrm{cell}}$ implies the initial condition for $\eta(0,t)$ for the integration of the differential equation system. The solution method is described in the next section.

2.3. Laplace-transformation of the governing equations

To calculate an impedance spectrum, each solution variable of the system of the differential equations (Eqs. (8)–(14)) is perturbed about a steady-state solution. For a small perturbation, the response of the system can be deduced from the Taylor expressions limited to the first order. Introducing these Taylor expressions in Eqs. (8)–(14) and subtracting the steady-state equations, we obtain a Laplace-transformed system of differential equations depending on frequency. The time-dependent perturbed variables are denoted with a bar, variables without a bar are the steady-state solutions and $s = \mathrm{i}\omega$ is the complex frequency.

According to Springer et al. [2], an approximate analytical transfer function (Eq. (15)) for the dynamic response of the oxygen mole fraction $\overline{x_{\mathrm{O_2}}}(y = l_{\mathrm{B}}, s)$ at the interface between the backing and the catalyst layer can be found depending on the dynamic response of the ionic current density $\overline{j_{\mathrm{cell}}}(s)$ and the steady-state oxygen mole fraction $x_{\mathrm{O_2}}^{\mathrm{gas}}$. This equation is used for the coupling of the backing with the catalyst layer in the frequency domain

$$\overline{x_{\mathrm{O_2}}}(l_{\mathrm{B}},s) = \frac{\overline{j_{\mathrm{cell}}}(s)}{i_{\mathrm{B}}} \frac{x_{\mathrm{O_2}}(l_{\mathrm{B}}) - \beta_1}{G(x_{\mathrm{O_2}}(l_{\mathrm{B}}))} \times \left(\tanh \frac{\sqrt{s\,\beta_1\, l_{\mathrm{B}}^2 / G(x_{\mathrm{O_2}}(l_{\mathrm{B}}))\, D_{\mathrm{eO_2N_2}}}}{\sqrt{s\,\beta_1\, l_{\mathrm{B}}^2 / G(x_{\mathrm{O_2}}(l_{\mathrm{B}}))\, D_{\mathrm{eO_2N_2}}}} \right). \tag{15}$$

Laplace-transformation of Fick's first law describing the diffusion of dissolved oxygen into an agglomerate yields:

$$\overline{j_{\mathrm{O_2}}^{r}}(r,y,s) = -D\left(c^* \frac{\partial \overline{c(r,y,s)/c^*}}{\partial r} + \overline{c^*} \frac{\partial (c(r,y)/c^*)}{\partial r} \right), \tag{16}$$

where $\overline{c(r,y,s)}/c^*$ denotes the dynamic response of the normalised local oxygen concentration.

The Laplace-transformed mass balance equation reads:

$$\begin{aligned} &\frac{1}{r^2} \frac{\partial (r^2 \overline{j_{\mathrm{O_2}}^{r}}(r,y,s))}{\partial r} \\ &= -\frac{i_0^{\mathrm{V}}}{nF}\, p_{\mathrm{O_2}} \overline{\left(\frac{c(r,y,s)}{c^*} \right)} \exp\left(\frac{2.3\,\eta(y)}{b} \right) \\ &\quad - \frac{i_0^{\mathrm{V}}}{nF}\, \overline{p_{\mathrm{O_2}}} \left(\frac{c(r,y)}{c^*} \right) \exp\left(\frac{2.3\,\eta(y)}{b} \right) \\ &\quad - \frac{i_0^{\mathrm{V}}}{nF}\, p_{\mathrm{O_2}} \left(\frac{c(r,y)}{c^*} \right) \frac{2.3}{b} \exp\left(\frac{2.3\,\eta(y)}{b} \right) \\ &\quad \times \bar{\eta}(y,s) - c^* s \overline{\left(\frac{c(r,y,s)}{c^*} \right)}, \end{aligned} \tag{17}$$

where the dynamic response of the oxygen partial pressure is given by $\overline{p_{\mathrm{O_2}}} = \overline{x_{\mathrm{O_2}}}(l_{\mathrm{B}}, s)\, P_{\mathrm{a}}$.

For the charge balance equation inside an agglomerate we obtain:

$$\begin{aligned} &\frac{1}{r^2} \frac{\partial (r^2 \overline{j_{\mathrm{p}}^{r}}(r,y,s))}{\partial r} \\ &= -i_0^{\mathrm{V}}\, p_{\mathrm{O_2}} \overline{\left(\frac{c(r,y,s)}{c^*} \right)} \exp\left(\frac{2.3\,\eta(y)}{b} \right) \\ &\quad - i_0^{\mathrm{V}} \overline{p_{\mathrm{O_2}}} \frac{c(r,y)}{c^*} \exp\left(\frac{2.3\,\eta(y)}{b} \right) \\ &\quad - i_0^{\mathrm{V}}\, p_{\mathrm{O_2}} \frac{c(r,y)}{c^*} \frac{2.3}{b} \exp\left(\frac{2.3\,\eta(y)}{b} \right) \bar{\eta}(y,s). \end{aligned} \tag{18}$$

The boundary conditions for Eqs. (16)–(18) are as follows:

- there is no variation of the dynamic response of the normalised oxygen concentration on the surface of the agglomerate $(\overline{c(R_{\mathrm{a}},y,s)}/c^*) = 0$,
- the gradient of the dynamic response of the normalised oxygen concentration in the centre of the agglomerates vanishes $\partial \overline{(c(0,y,s)/c^*)}/\partial r = 0$,
- the dynamic response of the current density vanishes in the centre of an agglomerate, i.e. $\overline{j_{\mathrm{p}}^{r}}(0,y,t) = 0$.

Inserting Eq. (16) into Eq. (17) and solving this differential equation, we obtain $\overline{\left(\frac{c(r,y,s)}{c^*}\right)}$ as a function of $\bar{\eta}(y,s)$ and $\eta(y)$. Inserting this expression for $\overline{\left(\frac{c(r,y,s)}{c^*}\right)}$ into Eq. (18), we obtain an analytical solution for the dynamic response of the current generation per agglomerate $\overline{j_{\mathrm{p}}^{r}}(R_{\mathrm{a}},y,s)$. The dynamic current response of the agglomerates is used to calculate the impedance of the entire cathode layer. Therefore, the differential equation system containing the Laplace-transformed charge balance equation in the y-direction (Eq. (19)) and Ohm's law (Eq. (20)) has to be solved.

$$\frac{\partial \overline{j_{\mathrm{p}}^{y}}(y,s)}{\partial y} = \overline{j_{\mathrm{p}}^{r}}(R_{\mathrm{a}},y,s)\Lambda + sC_{\mathrm{DL,V}}\bar{\eta}(y,s), \tag{19}$$

$$\frac{\partial\bar{\eta}(y,s)}{\partial y} = R_{\mathrm{Ohm}}\,\overline{j_{\mathrm{p}}^{y}}(y,s). \tag{20}$$

The boundary conditions are

- $\overline{j_{\mathrm{p}}^{y}}(0,s) = 0$: no variation of the current density at the backing/catalyst interface,
- $\bar{\eta}(0,s) = 1$: due to the linearity of the differential equation system, an arbitrary number not equal to zero can be chosen for $\bar{\eta}(0,s)$.

The cathode impedance $Z_{\mathrm{cath}}(\omega)$ at a frequency of ω is calculated by the quotient $\bar{\eta}(L,i\omega)/\overline{j_{\mathrm{p}}^{y}}(L,i\omega)$. For comparison with measured spectra the measured high frequency resistance R_{HF} is added to the cathode impedance

$$Z(\omega) = Z_{\mathrm{cath}}(\omega) + R_{\mathrm{HF}}. \tag{21}$$

We solve the differential equation system using *MATHEMATICA* 4®. The steady-state equations are solved as follows: the oxygen mole fraction at the backing/catalyst interface is determined by means of the implicit equation (Eq. (15)) for a given current density j_{cell}. With the knowledge of the dissolved oxygen concentration on the agglomerate surface (Eq. (9)), we obtain an analytical expression of the current generation per agglomerate as a function of the overpotential $\eta(y)$ (Eq. (12)). This term is used as a source term for the current density in the catalyst layer in Eq. (13). The differential equation system (Eqs. (13) and (14)) can be solved numerically using the function *NDSolve*. In doing so, the initial condition $\eta(0)$ is adapted using the Newton method (*FindRoot*) in order to obtain the second boundary condition $j_{\mathrm{p}}^{y}(L) = j_{\mathrm{cell}}$. The cell potential is calculated by

$$U_{\mathrm{cell}} = 1.23V - \eta(L). \tag{22}$$

NDSolve is a built-in function of *MATHEMATICA*® which finds numerical solutions of differential equations and systems using an Adams Predictor–Corrector method for non-stiff differential equations and backward difference formulae (gear method) for stiff differential equations. It switches between the two methods using heuristics based on the adaptively selected step size [14,15]. The results are given in terms of interpolating functions. Thus, we obtain the cell potential for a given current density and the distribution of the overpotential within the catalyst layer.

The catalyst layer equations in conjunction with the backing layer transfer function (Eq. (15)) are solved to calculate the cathode impedance Z_{cath}. *NDSolve* is used to solve the Laplace-transformed equations (Eqs. (19) and (20)). Because of the interaction between the backing layer and the catalyst layer, the value $\overline{j_{\mathrm{p}}^{y}}(L,s)$ has to be adapted iteratively using the Newton method (*FindRoot*) so that a self-consistent solution to the backing transfer function is found, i.e. $\overline{j_{\mathrm{p}}^{y}}(L,s) = \overline{j_{\mathrm{cell}}}(s)$.

3. Experimental

A small test fuel cell was constructed to validate our agglomerate model. To guarantee homogeneity in current density, temperature and gas supply over the whole MEA, the geometric active area is only 1.4 cm ×1.4 cm. The cell temperature can be controlled by water channels in the graphite plates that contain the flow-field. Serpentine flow-fields were machined in the graphite plates on both the anode and the cathode side. An untreated gas diffusion layers of type $TORAY^{®}TGP-H-120$ were utilised. A commercial MEA from GORE™ (PRIMEA® Series 5510, membrane thickness 25 μm) was investigated. The cell was connected to a Solartron 1286 electrochemical interface in combination with a Solartron 1255 HF frequency response analyser. The impedance spectra were measured in the frequency range between 0.1 Hz and 10 kHz. All ac impedance spectra were measured between the cathode and the anode, i.e. without a reference electrode. The gas flow was regulated with a gas flow controller, with the flow rate set to 110 sccm for hydrogen and 200 sccm for air at atmospheric pressure. Dry hydrogen was used on the anode side, on the cathode side the air was humidified with a wash bottle to 100% relative humidity (RH) at room temperature (20 °C). The measurements were made at a cell temperature of 39 °C. At this temperature the cathode gas has a RH of 33.4%.

The cell potentials of all polarisation curves mentioned in the text are corrected for the ohmic drop in the membrane. To determine the resistance of the membrane we used the real part of the 10 kHz impedance. For the parameter extraction all observed currents were corrected for an estimated crossover current of 7 A m^{-2} [16].

4. Comparison of measurements and simulation

The dotted lines in Fig. 3 shows measured impedance spectra in the potential range between 0.75 and 0.5 V. The high-frequency resistance decreases with decreasing cell potential. This can be explained by a change of the MEA water content. At low cell potential, i.e. with higher current densities, the product water humidifies the MEA leading to a smaller protonic resistance.

To validate our model, we searched for a set of parameters such that the model reproduces both measured impedance spectra at different current density values and the experimentally observed polarisation curve. The following parameters were fixed during the fitting procedure:

- The thickness of the catalyst layer was extracted from a microscope image to be $l_{\mathrm{c}} = 10\,\mu\mathrm{m}$.
- The diffusion coefficient of dissolved oxygen in an agglomerate D is set to $2 \times 10^{-9}\,\mathrm{m^2\,s^{-1}}$, according to Springer et al. [4]
- A gas diffusion layer with a thickness of 370 μm was used in the experiment. It is assumed that the thickness of the gas diffusion layer is reduced to $l_{\mathrm{B}} = 350\,\mu\mathrm{m}$ due to the contact pressure applied to the cell, thus the latter value was used for the simulation.

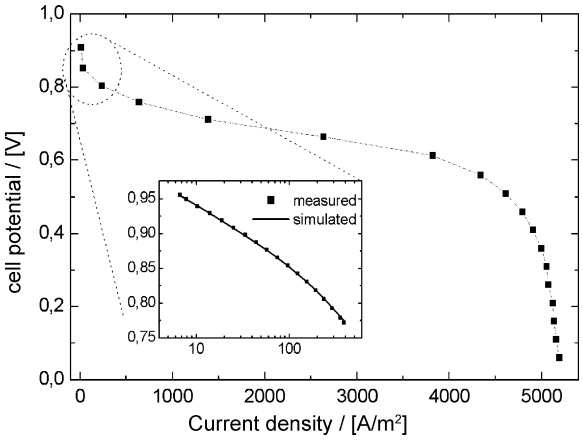

Fig. 2. Measured and simulated polarisation curves for low current density. The simulation shows good agreement with the measurement. A change of the apparent Tafel slope is obtained.

- The value of the agglomerate radius ($R_a = 0.1\,\mu m$) was adopted from Ihonen et al. [5].
- A value of 6.5 is chosen for the backing tortuosity τ (Springer et al. [2]$\tau = 7$).
- During the measurement, the operating pressure P_a was 1 atm (pressure drop in the flow-field is negligible) and the cell temperature was controlled to be 312 K.

Beginning with a comparison of the measured and simulated polarisation curves for low current density values results in a Tafel slope b of 78.3 mV and a volumetric exchange current density i_0^V of $7.74 \times 10^5\,A\,m^{-3}$ (see Fig. 2). Mass-transport limitations of dissolved oxygen into the agglomerates start already at low current density values indicated by the observed doubling of the apparent Tafel slope. The polarisation curve show also a sudden drop of the cell potential in the high current density range. This mass-transport limitation starting at the cell potential of 550 mV is attributed to flooding effects in the GDL and CL. For the following calculations these two parameter values were hold constant. We fitted the computed impedance spectra to the measured spectra in the range of low current density values ($639\,A m^2$, $1388\,A m^2$), where the spectra are not affected by oxygen diffusion limitation in the backing layer. Therefore, the backing layer parameters have no influence on the spectra under these operation conditions.

The fit parameters are Λ, R_{Ohm} and $C_{DL,V}$. Each parameter reveals a characteristic influence on the frequency-dependent shape of the simulated impedance spectrum. Moreover, the parameter influence on a simulated impedance spectrum changes depending on the overpotential. Therefore, the values of the parameters can be extracted by simultaneously fitting several simulated spectra to measured impedance spectra that correspond to different overpotential values. We obtain the best fit with a value of Λ of $35{,}000\,m^{-1}$. For further fits with higher current density values, where the spectra are affected by the diffusion limitation of the backing, we fixed the value of Λ and added the backing porosity ϵ_B as fit parameter to R_{Ohm}, $C_{DL,V}$.

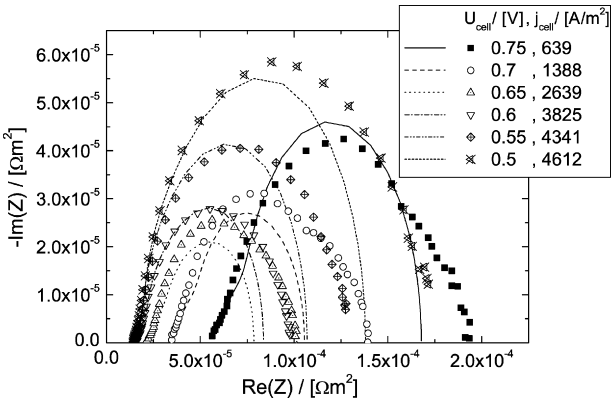

Fig. 3. Comparison between simulated (lines) and measured (dots) spectra for different current densities from $639\,A\,m^{-2}$ to $4612\,A\,m^{-2}$.

Fig. 3 shows the simulated and measured spectra for different current density values from $639\,A\,m^{-2}$ to $4612\,A\,m^{-2}$. Experimentally, the diameter of the impedance arc decreases with increasing current density due to a reduced charge transfer resistance for higher overvoltages. At a current density value of $2600\,A\,m^{-2}$ the measurement reveals a minimum value of the radius of the impedance arc, indicating that the charge transfer resistance is not longer the dominating loss mechanism. Subsequently the radius grows again as the current density increases. Oxygen mass-transport limitations are the main loss in this current density range. This characteristic behaviour of the impedance arcs is reproduced by our model. The simulated impedance spectra show good agreement with the measured spectra in the high and medium frequency range. The simulated impedance values for low frequency are too small. The measured impedance spectra reveal an additional mass-transport resistance that is not accounted for by our model. For instance, this could be diffusion limitation of gaseous oxygen in the open gas pores or the anodic impedance [17].

Fig. 4 shows the normalised values of the measured high frequency resistance R_{HF} and the normalised fit results of R_{Ohm} and $C_{DL,V}$ for different current density values. The maximum values used for the normalisation can be found in Table 1. It can be clearly seen that the measured high frequency resistance R_{HF},

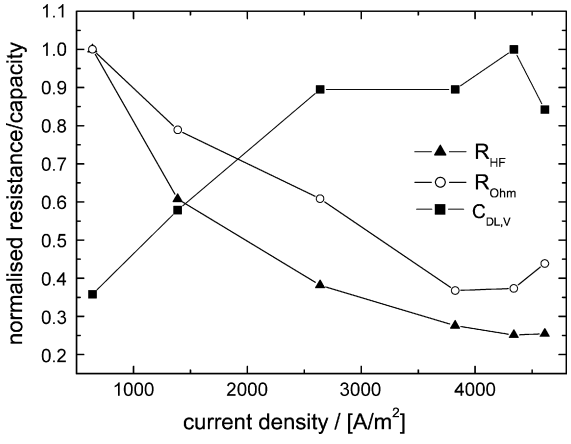

Fig. 4. Normalised values of the measured high frequency resistance R_{HF} and the normalised fit results of R_{Ohm} and $C_{DL,V}$ for different current density values.

Table 1
Maximum value of the high frequency resistance (HFR), the catalyst layer resistance (R_{Ohm}) and the double layer capacity ($C_{DL,V}$) used for the normalisation in Fig. 4. The HFR is experimentally measured and R_{Ohm} as well as $C_{DL,V}$ are obtained from the fit procedure.

High frequency resistance ($\times 10^{-5}\ \Omega\ m^2$)	5.6
Catalyst layer resistance (Ω m)	5.49
Double layer capacity ($\times 10^7\ F\ m^{-3}$)	1.9

Table 2
Parameters obtained from the fit procedure

b (V)	78.3
i_0^V (Am^{-3})	7.74×10^5
Λ (m^{-1})	35,000
R_{Ohm} $(\Omega\ m)$	2.02–5.49
$C_{DL,V}$ (Fm^{-3})	6.8×10^6–1.9×10^7

contributing mainly from the membrane, corresponds to the fitted ohmic resistance of the catalyst layer R_{Ohm}. For low current density, the water generation due to the ORR is not sufficient for a high stoichiometric air flow. This leads to a dehumidification of the MEA and thus to a decrease of the ionic conductivity in the catalyst layer and in the membrane. The humidification level of the MEA increases with increasing current density, leading to an decrease of R_{Ohm} and R_{HF}. Additionally, a better humidification of the electrode leads to a higher volumetric double-layer capacity $C_{DL,V}$, indicating an increase of the three-phase boundary.

At high current density the impedance spectra show no change in the high frequency resistance, indicating that the membrane is well humidified. Flooding occurs in the region of the limiting current density. The open pores become filled with liquid water so that the open pore space available for gas flow decreases. By setting the backing porosity ϵ_B to an value of 13%, we are able to fit the spectra at high current density values. This unrealistic value of ϵ shows that our one-phase model is not valid for values near the limiting current density if liquid water is present in the porous media. The parameter obtained from the curve fitting are summarized in Table 2. A fuel cell model that covers the whole range of current density values from zero to limiting current density without changing model parameters has to include the water management. The simulation of flooding effects and dehydration of the ionomer are essential for the interpretation of experimental data. The implementation of a transport equation for liquid water in the porous media (GDL, CL) coupled with water film formation around the agglomerates lowering the oxygen diffusion to the active sides and the description of the water content in the ionomer which contribute to a change in the proton conductivity and activity [18] is ongoing work.

5. Parameter study

This section presents an investigation of the effect of the cathode parameters on the shape of the polarisation curves and the impedance spectra. The parameter study outlined here helps to interpret measurement results and to analyse the influence of the cathode parameters on the shape of the curves within different measurement regimes.

5.1. Polarisation curves

The parameter study was performed by varying each model parameter by about ±50% with respect to the following baseline case: $b = 53$ mV, $R_a = 0.1\ \mu$m, $D = 5 \times 10^{-10}\ m^2\ s^{-1}$, $i_0^V = 15.2 \times 10^4\ Am^{-3}\ atm^{-1}$, $l_c = 10\ \mu$m, $\Lambda = 5 \times 10^3\ m^{-1}$. Due to the strong influence of the Tafel slope on the polarisation curve, this parameter was only varied by about ±10% of the baseline case value.

First the effect of the Tafel slope is studied. Fig. 5(a) shows simulated polarisation curves for three different values of the Tafel slope. As mentioned before, the curves show a strong response to the change of the Tafel slope over the whole current density range. A doubling of the apparent Tafel slope is observed in all cases.

At low current density values, the performance of the cathode depends strongly on the agglomerate radius (Fig. 5b). Here, the ORR occurs within the entire volume of the agglomerate. Diffusion limitation does not occur here. An increase of the agglomerate radius causes an increase of the reaction volume. The diffusion limitation is more pronounced for a higher agglomerate radius. The doubling of the Tafel slope can be observed at a lower current density in this case.

Fig. 5(c) shows the dependence of the polarisation curve on the diffusion coefficient of dissolved oxygen into the agglomerates. For low current density, the oxygen diffusion inside the agglomerates is not a limiting effect. Thus, the polarisation curves corresponding to low current density do not depend on the diffusion coefficient. In this case, the whole agglomerate is supplied by oxygen and utilised for the ORR. The diffusion coefficient determines the current density value where the diffusion limitation occurs and the apparent Tafel slope changes. A smaller diffusion coefficient causes a shift to smaller values of the current range corresponding to the doubling of the Tafel slope.

The exchange current density is varied in Fig. 5(d). An increase of the exchange current density shifts the polarisation curves to lower overpotential. No influence on the doubling of the apparent Tafel slope is observed.

The product Λ of the agglomerate surface area and the density of the agglomerates and the thickness of the catalyst layer L have almost the same influence on the polarisation curves (Fig. 6). Both a thickness increase of the catalyst layer (Fig. 6a) and an increase of Λ (Fig. 6b) lead to a higher volume that is available for the ORR. Consequently, more current can be generated in the catalyst layer at the same overpotential.

An influence of the backing layer parameters on the polarisation curve is only evident at high current density. Here, oxygen diffusion through the backing is limiting the fuel cell performance. Accumulation of condensed liquid water determines the saturation in the gas diffusion layer. As explained in Section 4, this effect can be interpreted as a decrease of the effective porosity of the gas diffusion layer in our model.

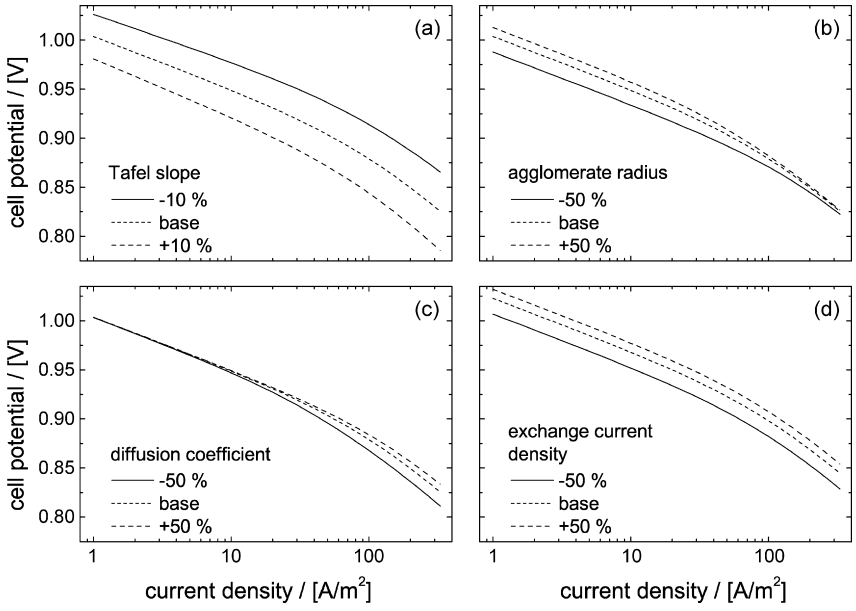

Fig. 5. Parameter variations show the influence on the doubling of the apparent Tafel slope. (a) Variation of the Tafel slope, (b) variation of the agglomerate radius, (c) variation of the diffusion coefficient, (d) variation of the exchange current density.

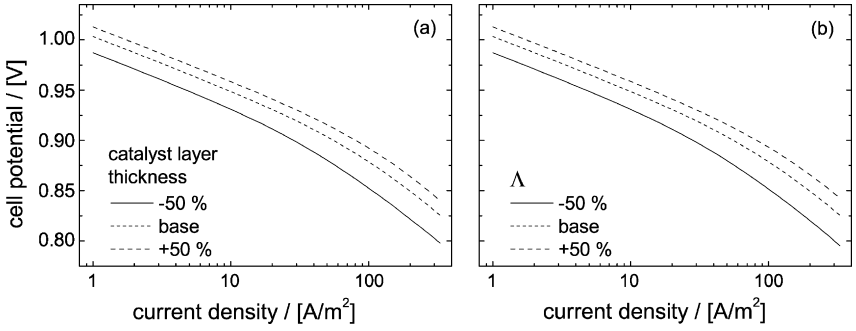

Fig. 6. Variation of the thickness of the catalyst layer (a) and of the ratio of the agglomerate surface area to unit volume (b) shows a similar influence.

5.2. Impedance spectra

Fig. 7 shows the effect of varying the ionic resistance in the catalyst layer. The spectra are calculated at a current density of 639 A m^{-2}. The higher the ionic resistance of the catalyst layer, the more distinct is the linear branch with an angle of 45° between the real axis and the impedance plot in the Nyquist representation. This branch reflects coupling of the distributed ionic resistance and the distributed capacitance of the catalyst layer. That is, the double-layer charging effects and the proton transport dominate the overall electrode response in the high-frequency regime [2,19].

Fig. 8(a) shows simulated impedance spectra for different current density values. The parameters of the baseline case are close to the validated parameter values (Table 2). For low current density values the spectrum is determined by the ORR, indicated by the decrease of the Nyquist arc radius with increasing overpotential. This behaviour changes for high current

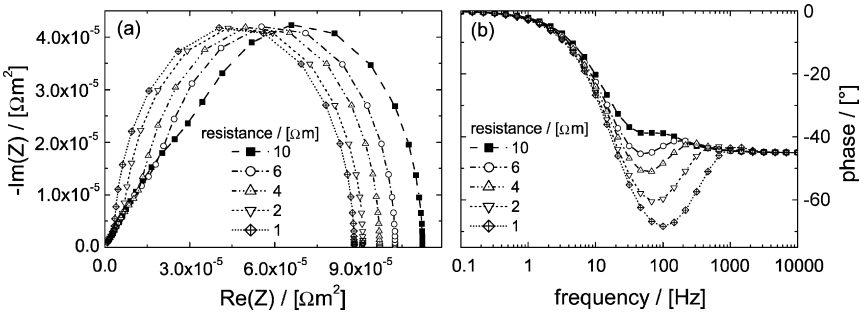

Fig. 7. The influence of the ionic resistance in the catalyst layer on the impedance is shown.

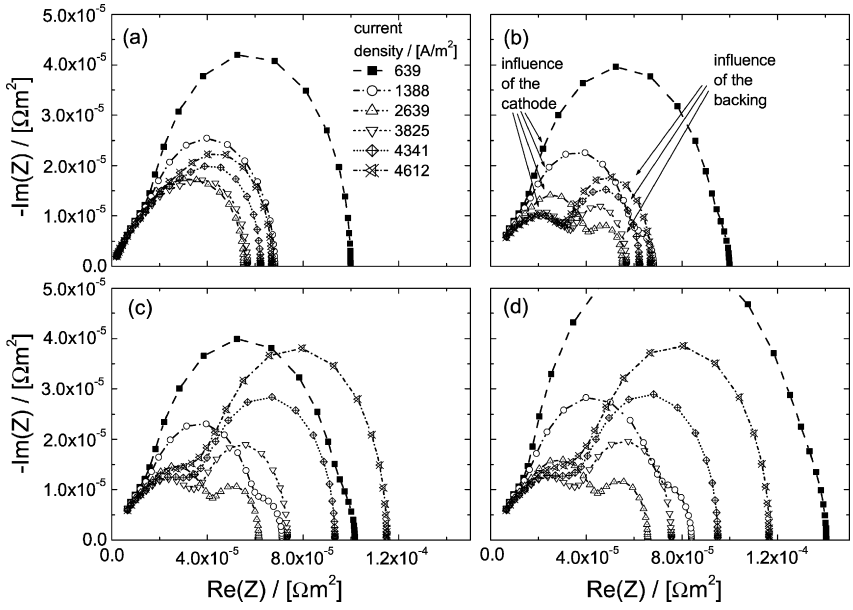

Fig. 8. Investigation of the processes that dominates the shape of the impedance spectra. (a) Baseline case, (b) reduced: $C_{DL,V}$, (c) reduced: $C_{DL,V}$ and ϵ_B, (d) reduced: D.

density values where the radius of the Nyquist arc increases with increasing overpotential, indicating that the charge transfer resistance is not longer the dominating loss mechanism. To understand this change we reduced the volumetric double-layer capacity $C_{DL,V}$ from $10^7\,Fm^{-3}$ to $10^6\,Fm^{-3}$ in Fig. 8(b) without changing other parameters. Two separate arcs appear at higher current density values. The high-frequency arc corresponding to the ORR decreases with increasing overpotential. The low-frequency arc increases with increasing overpotential. This arc corresponds to the backing impedance. Fig. 8(c) shows the same spectra like in Fig. 8(b) but simulated with an additional lower effective backing porosity, changed from 0.14 to 0.12. The lowered backing porosity does not influence the high-frequency arc but the radius of the low-frequency arc is enlarged at high current density compared to the low-frequency arc in Fig. 8(b). In addition, Fig. 8(d) shows impedance spectra with a minimised diffusion coefficient for oxygen inside the agglomerates from $5 \times 10^{-9}\,m^2 s^{-1}$ to $5 \times 10^{-10}\,m^2\,s^{-1}$ ($C_{DL,V}$ has still the reduced value of $10^6\,Fm^{-3}$). Now, the high-frequency arc expands due to diffusion limitation in the agglomerates. From the results of Fig. 8 it can be concluded that a high volumetric double-layer capacity masks the two distinct arcs (like in the case of our investigated MEA) and therefore the loss mechanism cannot separated easily. Depending on the current density either the first high frequency arc or the second low-frequency arc, which are merged to one arc in case of a high double-layer capacity, dominates the overall impedance spectrum and therefore the radius decreases or increases with increasing overpotential. This explains the shape of the measured impedance spectra at different operation points.

5.3. Sensitivity analysis

By means of parameter variation, the influence of the model parameters on the impedance spectra at different current density values was investigated. The behaviour of the impedance spectra once with low current density ($639\,A\,m^{-2}$) and once with high current density ($4341\,A\,m^{-2}$) were tested. The validated parameter set was selected as a baseline case. Each parameter was varied about ±10% in comparison to the baseline value. The parameters of the gas diffusion layer have no influence on the impedance spectra at low current density. This statement is certainly only valid, as long as the parameter values of the gas diffusion layer (GDL) do not give rise to a limiting current in the low current density region.

In the low current density range, the electrode dominates the shape of the impedance spectra: a reduction of the product Λ of the agglomerate surface area and the density of the active agglomerates in the catalyst layer, a reduction of the diffusion coefficient of dissolved oxygen in the agglomerates D or an increase of the agglomerate radius R_a cause an increase of the diameter of the impedance arc. At low current density values, the variable $\bar{c}$ dominates the Eqs. (17) and (18), which are linked to the diffusion constant and the agglomerate radius by Eq. (16).

In the high current density range, the parameters of the gas diffusion layer dominate the shape of the impedance spectra. The backing parameters determine the current density at which diffusion limitation in the GDL occurs. Thus an increase of the thickness of the gas diffusion layer l_B or the tortuosity τ or a reduction of the backing porosity ϵ_B leads to an increase of the diameter of the impedance arc at high current density values.

This effect can be explained by means of Eqs. (17) and (18). The dynamic response of the oxygen partial pressure $\overline{p_{O_2}}$ dominates the sink terms of the differential equations at high current density. $\overline{p_{O_2}}$ is linked to the transfer function for the dynamic response of the oxygen mole fraction (Eq. (5) in [2]) by the relationship $\overline{p_{O_2}} = \overline{x_{O_2}}\,P_a$ and consequently to the model parameters of the GDL.

The Tafel slope b has a strong influence on the shape of the impedance spectra over the whole current density range. An increase of the Tafel slope causes an increase of the diameter of the impedance arc.

This can also be explained by means of Eqs. (17) and (18). On the right-hand side of Eqs. (17) and (18), there is an exponential function with the Tafel slope in each addend. Thus, the Tafel slope always has a strong influence on the shape the impedance spectra, regardless of which Laplace-transformed function is dominating the equation.

It was found that the volumetric exchange current density i_0^{V} does not affect the spectrum. Due to the characteristic of the differential equation system the exchange current density i_0^{V} only affects the absolute value of the overpotential η but not the shape of its distribution in the catalyst layer for a given current density value. Due to the fact that only the product of $i_0^{\mathrm{V}}\ \exp(2.3\eta/b)$ appears in Eqs. (17) and (18), a change in i_0^{V} does not affect the impedance because the product remains unchanged. A mathematical explanation of this fact can also be found in Jaouen et al., Appendix B [9]. The volumetric exchange current density only affects the current–voltage characteristics and can therefore only be extracted on polarisation curves.

A larger oxygen gas pressure at the inlet improves the reaction due to a higher dissolved oxygen concentration in the agglomerates. Therefore, the diameter of the impedance arc decreases.

Variation of the volumetric double-layer capacity $C_{\mathrm{DL,V}}$ over a small range does not change the shape of the impedance spectrum in the Nyquist representation. In the Bode representation, one recognises a phase shift of the peak of the absolute impedance values towards lower frequencies by increasing the capacity. For a very low double-layer capacity at high current density two separate arcs occur in the Nyquist plot (see Fig. 8).

In the high-frequency range, the ionic resistance R_{Ohm} and the thickness of the catalyst layer l_{c} affect the 45° branch, and therefore also the regime of the impedance spectra at low frequencies (see Fig. 7).

There are additional parameters in the model, that influence the shape of the impedance spectra in a similar way:

- The product Λ of the agglomerate surface area and the density of the active agglomerates in the catalyst layer, the diffusion coefficient of the dissolved oxygen in an agglomerate D and the agglomerate radius R_{a} have the same influence on the simulated impedance spectra:

  $$\Lambda \leftrightarrow D \leftrightarrow R_{\mathrm{a}}.$$

- Likewise, the influence of the tortuosity τ, porosity ϵ_{B} and the thickness of the gas diffusion layer l_{B} can hardly be distinguished:

  $$\tau \leftrightarrow \epsilon_{\mathrm{B}} \leftrightarrow l_{\mathrm{B}}.$$

Therefore, ex situ measurements are required to determine parameters like porosity and the mean radius of the agglomerates, e.g. porosimetry measurement of the GDL and STEM plots of the cathode.

6. Conclusion

A one-dimensional cathode agglomerate model for analysing impedance spectra was developed and validated with experimental data. The model predicts the measured doubling of the apparent Tafel slope, which occurs due to diffusion limitation of dissolved oxygen into the agglomerates. The model shows a good agreement in the characteristic behaviour of the measured impedance spectra at different current density values. In the low frequency range the model predicts a too low impedance in comparison with measured spectra. An explanation for this could be that the anodic impedance or the diffusion limitation of gaseous oxygen in the catalyst layer cannot be neglected.

The fitting results show that a better humidification of the electrode leads to a higher volumetric double layer capacity. The fitted ohmic resistance of the catalyst layer shows the same behaviour on the current density as the measured high frequency resistance due to product water humidifying the ionomer.

The influence of the model parameters on the polarisation curve and the impedance spectrum were investigated.

The implementation of a transport equation for liquid water in the porous media coupled with water film formation around the agglomerates lowering the oxygen diffusion to the active sides is ongoing work.

References

[1] T.E. Springer, S. Gottesfeld, in: Proceedings of the Symposium on Modeling of Batteries and Fuel Cells, vols. 91–10, The Electrochemical Society, 1991, pp. 197–208.
[2] T. Springer, T. Zawodzinski, M. Wilson, S. Gottesfeld, J. Electrochem. Soc. 143 (2) (1996) 587–599.
[3] J. Giner, C. Hunter, J. Electrochem. Soc. 116 (1969) 1124–1130.
[4] T. Springer, I. Raistrick, J. Electrochem. Soc. 136 (6) (1989) 1594–1603.
[5] J. Ihonen, F. Jaouen, G. Lindbergh, A. Lundblad, J. Electrochem. Soc. 149 (4) (2002) A448–A454.
[6] M.A. Al-Saleh, S. Gultekin, S. ur Rahman, A. Al-Zakri, J. Power Sources 55 (1) (1995) 33–39.
[7] M. Perry, J. Newman, E. Cairns, J. Electrochem. Soc. 145 (1) (1998) 5–15.
[8] F. Jaouen, G. Lindbergh, G. Sundholm, J. Electrochem. Soc. 149 (4) (2002) A437–A447.
[9] F. Jaouen, G. Lindbergh, J. Electrochem. Soc. 150 (12) (2003) A1699–A1710.
[10] A. Damjanovic, V. Brusic, Electrochim. Acta 12 (6) (1967) 615–628.
[11] A.S. Aricò, V. Alderrucci, V. Antonucci, S. Ferrara, V. Recupero, N. Giordano, K. Kinoshita, Electrochim. Acta 37 (3) (1992) 523–529.
[12] O. Antoine, Y. Bultel, R. Durand, J. Electroanal. Chem. 499 (2001) 85–94.
[13] P.W. Atkins, Physikalische Chemie, 3rd ed., Wiley–VCH, Weinheim, 2001.
[14] S. Wolfram, The Mathematica Book, Addison-Wesley Verlag, Germany, 1980.
[15] L. Petzold, SIAM J. Sci. Stat. Comput. 4 (1983) 136–148.
[16] S. Cleghorn, J. Kolde, W. Liu, in: W. Vielstich, H. Gasteiger, A. Lamm (Eds.), Handbook of Fuel Cell—Fundamentals, Technology and Applications, vol. 3, John Wiley and Sons, 2003, pp. 566–575.
[17] G. Li, P. Pickup, Electrochim. Acta 49 (2004) 4119–4126.
[18] K. Neyerlin, H. Gasteiger, C. Mittelsteadt, J. Jorne, G. Wenbin, J. Electrochem. Soc. 152 (6) (2005) A1073–A1080.
[19] E. Eikerling, A. Kornyshev, J. Electroanal. Chem. 475 (1999) 107–123.